Synchronization in air-slot photonic crystal optomechanical oscillators

Yongjun Huang,[1,2,a)] Jiagui Wu,[2,3] Jaime Gonzalo Flor Flores,[2] Mingbin Yu,[4] Dim-Lee Kwong,[4] Guangjun Wen,[1] and Chee Wei Wong[2,b)]
[1]*Centre for RFIC and System Technology, School of Communication and Information Engineering, University of Electronic Science and Technology of China, Chengdu 611731, China*
[2]*Fang Lu Mesoscopic Optics and Quantum Electronics Laboratory, University of California, Los Angeles, California 90095, USA*
[3]*College of Electronic and Information Engineering, Southwest University, Chongqing 400715, China*
[4]*Institute of Microelectronics, A*STAR, Singapore 117865*

(Received 11 January 2017; accepted 3 March 2017; published online 16 March 2017)

In this Letter, we report observations for the optomechanical oscillator (OMO) synchronization in an air-slot photonic crystal (PhC) cavity driven by a single laser source. Two very-close mechanical modes are found in the air-slot PhC OMO cavity and can be locked to each other at drive powers above the threshold with different detunings. The improvement in phase noise (−70 dBc/Hz at 10 kHz offset) for the synchronized OMO is reported as well. The stable frequency tones obtained open a path toward reconfigurable synchronized oscillator networks. *Published by AIP Publishing.* [http://dx.doi.org/10.1063/1.4978671]

Synchronization is a widely observed phenomenon in nature which, for example, can be found in pendulum clocks hanging on the same wall,[1] rhythmic flashes of light pulses in fireflies,[2] multiple-order synchronizations in a magnetic resonance laser,[3] ensembles of atoms,[4] and the biological clock in humans, animals, and plants.[5] Synchronization is of importance for the fundamental research as well as the practical application, such as in time-keeping,[6] signal processing and microwave communications,[7] and computing and memory concepts.[8,9]

Enabled by advances in nanofabrications, several observations on the synchronization in micro- and nanomechanical oscillators have been reported recently.[10–16] These include the exciting chip-scale optomechanical oscillator (OMO) platform.[10,12,14–17] Specifically, Zhang *et al.* obtained the synchronization in two dissimilar silicon nitride OMOs which are spaced by a few hundred nanometers,[10] and demonstrated that phase noise reduction was achieved in multiple OMO arrays.[15] Bagheri *et al.* then demonstrated that two mechanically isolated oscillators could be synchronized as well by a photonic resonator.[12] Quite recently, Shah *et al.* further demonstrated that two independent oscillators separated far from each other (3.2 km) could be coupled via light.[14] In addition, Li *et al.* theoretically analyzed the long-distance unidirectional synchronization can be obtained for more than two oscillators.[16] Moreover, theoretical analysis on the synchronization transition (in-phase and anti-phase) in two optomechanical oscillators was also reported.[18,19]

Those OMO systems are composed of two oscillators and more, and need strong enough intracavity laser drive power to achieve the synchronization. Here, we report on observations for the synchronization in an air-slot photonic crystal (PhC) OMO driven by a single laser source. The synchronization obtained in this paper is from two very-close mechanical modes in the same optomechanical cavity, which is quite different from the previously reported dual or multiple mechanical oscillators. Multiple mechanical modes[20] or dynamical control[21] also enable laser cooling approaches. Moreover, since the single air-slot PhC OMO exhibits higher optical Q and larger optomechanical coupling,[22–25] the optical power needed to obtain the synchronization in a wide optical detuning range is lower than previously reported OMO platforms, in terms of relationship:[25] $P_{th} \propto 1/\left(Q_o^3 Q_m g_0^2\right)$, where Q_o, Q_m, g_0 stand for the optical Q, mechanical Q, and optomechanical coupling, respectively. This helps to reduce the phase noise, as the measured single sideband phase noise of the free-running OMO indicates the noise level of −70 dBc/Hz at 10 kHz offset, which is the lowest level compared to the previously reported synchronized OMOs. It indicates a path toward reconfigurable high-performance synchronized oscillator networks.

Figs. 1(a)–1(c) show the optical image and zoom-in scanning electron microscopic (SEM) images of the examined air-bridged slot-type PhC cavity fabricated with 248 nm deep-UV lithography and reactive ion etching on 250 nm thickness silicon-on-insulator wafers (see Methods in our previous works[25] for more details). The localized slot guided mode is formed by first introducing a narrow air slot line-defect and shifting the center air holes by 15 nm (blue), 10 nm (green), and 5 nm (red), respectively, as shown in zoomed-in SEM image (Fig. 1(c)). A post-fabrication optical and mechanical modeling results based on these parameters are shown in Figs. 1(d) and 1(e),[22,23,25] which theoretically indicate the intrinsic optical quality factor to be approximately 500 000 with mode volume of approximately $0.07(\lambda/n_{air})$.[3] Such high quality factor to small mode volume (Q/V) ratio is important for observing OMO at low threshold powers.[25,26] We note that in Fig. 1(e) we only show the displacement for the fundamental mode, and it will be analyzed later; there is another mechanical mode very close to the fundamental mode. We also note that the optical and mechanical modelings are performed separately, so the optomechanical coupling effect is ignored.

The measurement setup for characterizing the optical resonance and mechanical resonance/self-sustaining oscillation is

a)Electronic mail: yongjunh@uestc.edu.cn
b)Electronic mail: cheewei.wong@ucla.edu

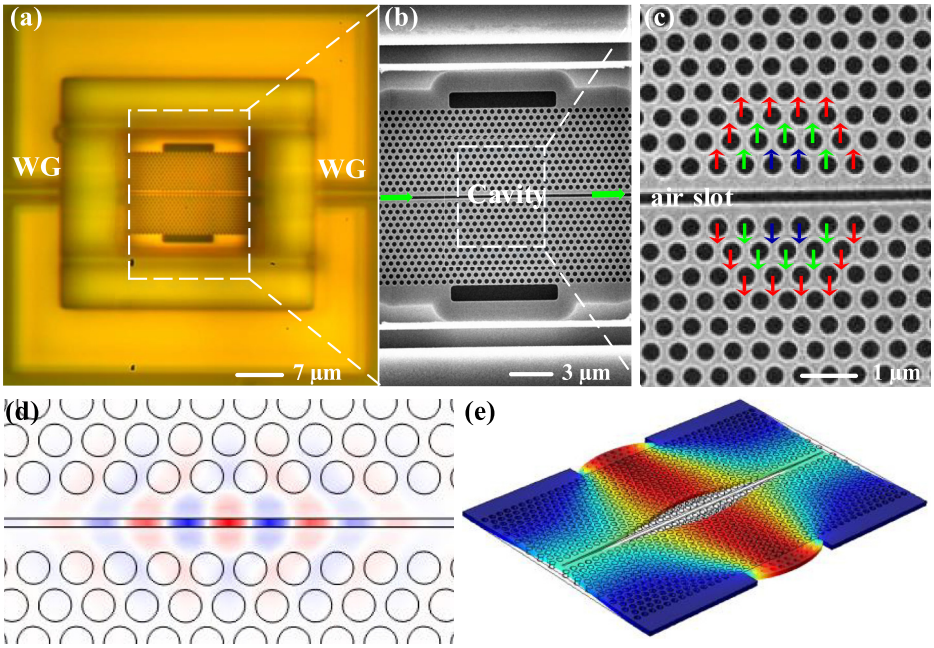

FIG. 1. (a) Optical image of designed optomechanical oscillator with inline input/output waveguides (WG). (b) Zoom-in scanning electron micrograph (SEM) of air-bridged photonic crystal slot cavity, along with optimized design input/output slot waveguide. The lattice constant is 510 nm and the ratio between hole radius and lattice constant is 0.3, centering the optical resonance within the photonic band gap and at 1550 nm. (c) Zoom-in SEM of the slot cavity, formed by the differential perturbative shifting of the nearest neighbor holes from a periodic lattice and denoted by the arrows. (d) Modelled *E*-field distribution of the optical resonances. (e) Modelled mechanical displacement for the fundamental eigenmode.

shown in Fig. 2(a). In our experiments, the optical quality factor is obtained and have typically loaded optical quality factors (Q_o) in the range of 60 000–100 000 (one Lorentzian fitted curve for the optical resonance at low laser drive power is shown in the inset of Fig. 2(b)). The modelled *E*-field distribution of fundamental slot-guided mode is shown in Fig. 1(d). It indicates that most of the light fields are concentrated in the air slot, creating a large gradient force pushing on the physical boundary of air slot. This leads to large zero-point optomechanical coupling strength ($g_0 \approx 800$ kHz)[25] with the fundamental mechanical mode (with an effective mass of 6.11 pg), as shown in Fig. 1(e) for mode displacement profile with the mechanical eigenfrequency of approximately 105 MHz. For most of our previously measurements,[23,25] only one mechanical mode is observed.

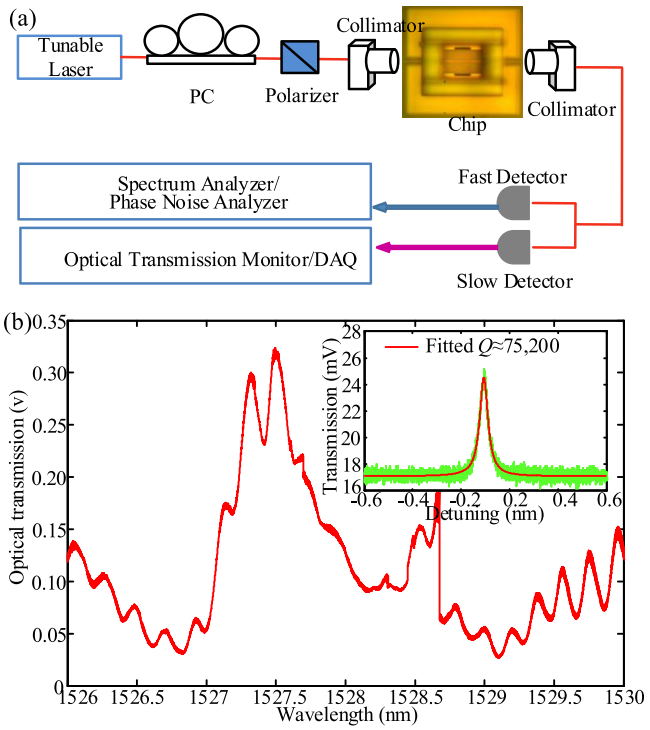

FIG. 2. (a) Simplified experimental setup for the optical transmission and mechanical resonance measurements of the examined OMO. (b) Measured optical transmission at 300 μW input drive laser power.

Here, we will show that we can also get two very-close mechanical modes, based on many different chips nanofabricated across the same wafer. To clearly see such two mechanical modes we drive the OMO with higher laser power at ~300 μW (the estimated oscillation threshold power is ~127 μW[25]). The corresponding optical transmission is shown in Fig. 2(b), which clearly shows the thermal nonlinearity. Then we collect the mechanical power spectral density (PSD) with the photodetector while changing the laser pump wavelength from 1527 nm to 1528.8 nm (and hence the laser-cavity detuning) with steps of 5 pm, through Labview programs. The corresponding two-dimensional results are shown in Fig. 3(a). Here a RF signal analyzer (Agilent N9000A CXA) is used to capture the transduced mechanical power spectral densities, and the resolution bandwidth (RBW) is set as 20 kHz.

As can be seen in Fig. 3(a), different regions are obtained wherein we can characterize them as a solely mechanical resonance state, chaos state,[27] sub-harmonics generation state,[25,28] self-pulsation oscillation (SPO) state,[29] and the synchronized state. Here, we will not focus on the variety of states shown in Fig. 3(a) as some have been discussed elsewhere,[27,28] but instead concentrate on the observed two mechanical modes and the resulting synchronization. A zoom-in plot is presented in Fig. 3(b) for more details on the dynamics. The RBW of the Agilent N9000A CXA signal analyzer here is set as 3 kHz. It clearly shows that two mechanical modes located at 105.5 MHz and 107.1 MHz are obtained. We can see the synchronization appears after the laser detuning larger than 1527.5 nm and the mechanical resonance is transferred to self-sustaining oscillation because the intrinsic mechanical losses are dwarfed by the optomechanical amplification.[26] The stiffened mechanical oscillation frequency arises from the optical spring effect, on top of the solely RF resonance.

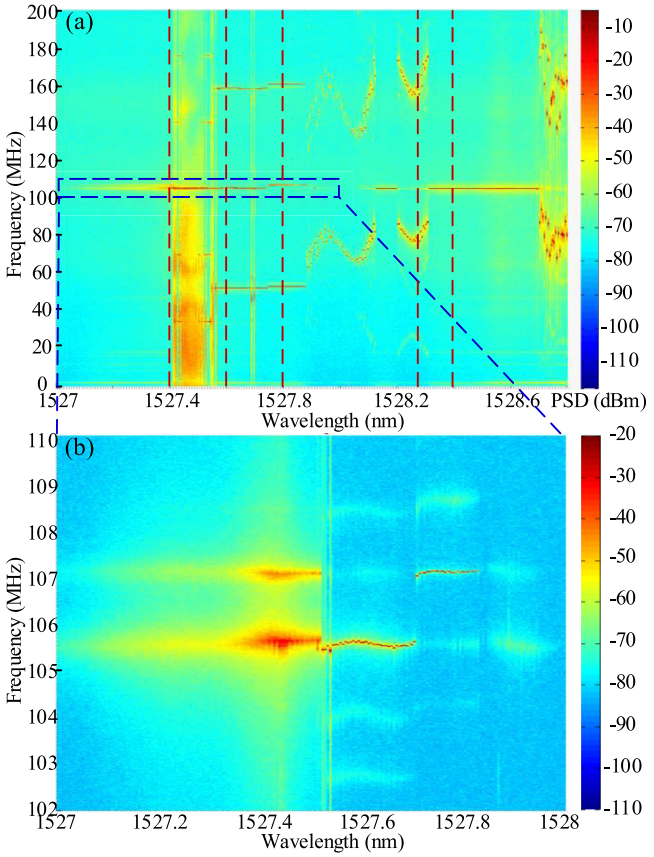

FIG. 3. (a) Collected mechanical power spectral densities at different laser detunings from 1527 nm to 1528.8 nm. (b) Zoom-in plot for better visualization of the two mechanical modes, collected in another experimental run.

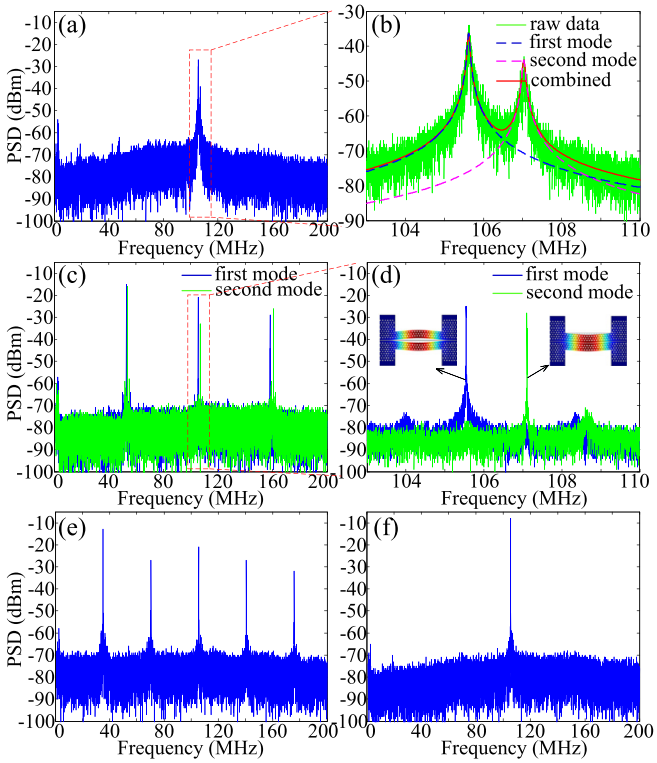

FIG. 4. Measured mechanical RF power spectral density (PSD) at (a) and (b) 1527.4 nm, (c) and (d) 1527.6 nm (blue), and 1527.8 nm (green), (e) 1528.25 nm, and (f) 1528.4 nm. Lorentzian fits are superimposed in panel (b) and the finite-element modelled displacements for the corresponding modes are inserted in panel (d).

Fig. 4 illustrates the mechanical power spectral densities at several key laser detunings (labeled in Fig. 3 with red dashed lines) to clearly show the features of mechanical modes. Specifically, before oscillation, the two mechanical modes are excited independently, and the Lorentz fitted mechanical quality factors are approximately 1960 and 1490 for such two modes, respectively. The quality factor of the first mode is larger than the second mode, so the self-sustaining oscillation of the first mode appears first, and the synchronized frequency tone is located at 105.5 MHz, as shown in Fig. 3. When the laser detuning is changed and the laser power exceeds the oscillation threshold of the second mechanical mode (estimated to be $\sim$144 μW), the synchronized frequency tone jumps to 107.1 MHz. The finite-element modelled mechanical displacements for the two modes are inserted in Fig. 4(d). We can know that both mechanical modes are in-plane modes and so can be coupled via the optical fields properly with similar optomechanical couplings. The only difference in the modes is that the displacement directions of the two suspended silicon membranes are in a differential mode (first mode; exactly out-of-phase) and a common mode (second mode; in-phase). It should be noticed that the in-phase and out-of-phase mode transitions in our OMO are different from the previous theoretical analysis for in-phase and anti-phase transitions between two oscillators.[18,19] Moreover, one power spectral density with the laser detuning of 1528.25 nm is shown in Fig. 4(e) for the self-pulsation oscillation (SPO) state. The frequency tones located around 52 MHz and 157 MHz in Fig. 4(c) are the subharmonics due to the intracavity locking between OMO and SPO,[25] and the frequency tone around 160 MHz in Fig. 4(e) is the first order harmonic of SPO. When continuing to increase the laser wavelength, the synchronized frequency tone returns to 105.44 MHz and one mechanical power spectral density with the laser detuning of 1528.4 nm is shown in Fig. 4(f) which indicates the largest signal-to-noise ratio.

Finally, to characterize the stability of the synchronized frequency tones, we carry out the phase noise measurements by using an Agilent E5052A signal source analyzer, and the measured results are shown in Fig. 5 for both synchronized states corresponding to the two curves shown in Fig. 4(d). The inset in Fig. 5 is the corresponding zoom-in mechanical RF power spectral density at laser detuning of 1527.8 nm, which indicates the narrow linewidth of the self-sustaining oscillation state. It can be seen that both synchronized frequency tones have very good phase noise performances. The second synchronized state has 2 dB phase noise reduction in the frequency offset up to 10 kHz, due to the smaller noise performance which can also be found in Fig. 4(d). By the closed-loop Leeson model,[30] the synchronized frequency tones have $1/f^3$ flicker frequency noise below 1 kHz, $1/f^2$ white frequency noise in the range of 1 kHz to 4 MHz, and $1/f^0$ white phase noise at higher frequency offsets. The Leeson frequency (f_L) and corner frequency (f_c) are then obtained through a power law fit[30] of the phase noise plot as $f_L = 1$ kHz and $f_c = 4$ MHz, respectively. It should be noted that the obtained free-running phase noise is about -70 dBc/Hz at 10 kHz offset, which is lower than the synchronized frequency tone obtained in prior multiple resonator studies.[15]

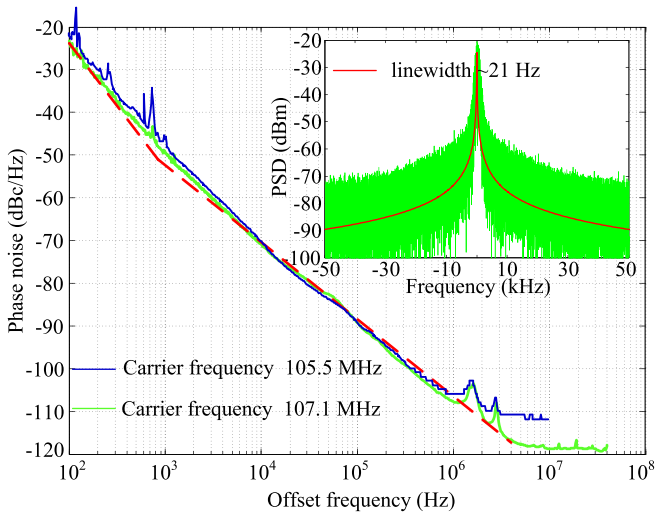

FIG. 5. Measured phase noises for the two synchronized frequency tones of 105.5 MHz and 107.1 MHz at the corresponding pump laser wavelength of 1527.6 nm and 1527.8 nm. Inset is the zoom-in mechanical PSD for the second synchronized mode with Lorentzian fit which shows the narrow linewidth of the self-sustaining oscillation state. Here, RBW is set as 1 Hz.

In this Letter, synchronization phenomena are observed and characterized in an air-bridged slot-type PhC OMO. Two very-close mechanical modes are found in the single air-slot PhC OMO cavity and can be locked to each other at driving powers above the threshold with different detunings. This is different from the previously reported synchronization results obtained in dual or multiple resonators. The measured phase noise for the synchronized OMO is presented and good performance is obtained, which indicates a path toward reconfigurable synchronized oscillator networks.

The authors acknowledge the discussion with Shu-Wei Huang and Jinkang Lim. Chip fabrications were carried out at the Institute of Microelectronics in Singapore. This work was supported in part by the Office of Naval Research under Grant (N00014-14-1-0041), the Defense Advanced Research Projects Agency (DARPA) DSO optomechanics program under Grant No. FA9550-10-1-0297—C11L10831, and the National Natural Science Foundation of China (Grant Nos. 61371047 and 11474233).

[1]C. Huygens, *Horologium Oscillatorium* (Apud F. Muguet, Paris, France, 1673).
[2]J. Buck and E. Buck, Science **159**, 1319 (1968).
[3]J. Simonet, M. Warden, and E. Brun, Phys. Rev. E **50**, 3383 (1994).
[4]M. Xu, D. A. Tieri, E. C. Fine, J. K. Thompson, and M. J. Holland, Phys. Rev. Lett. **113**, 154101 (2014).
[5]A. Pikovsky, M. Rosenblum, and J. Kurths, *Synchronization: A Universal Concept in Nonlinear Sciences* (Cambridge University Press, Cambridge, England, 2001).
[6]F. Sivrikaya and B. Yener, IEEE Network **18**, 45 (2004).
[7]S. Bregni, *Synchronization of Digital Telecommunications Networks* (Wiley, Chichester, 2002).
[8]I. Mahboob and H. Yamaguchi, Nat. Nanotechnol. **3**, 275 (2008).
[9]M. Bagheri, M. Poot, M. Li, W. P. H. Pernice, and H. X. Tang, Nat. Nanotechnol. **6**, 726 (2011).
[10]M. Zhang, G. S. Wiederhecker, S. Manipatruni, A. Barnard, P. McEuen, and M. Lipson, Phys. Rev. Lett. **109**, 233906 (2012).
[11]D. K. Agrawal, J. Woodhouse, and A. A. Seshia, Phys. Rev. Lett. **111**, 084101 (2013).
[12]M. Bagheri, M. Poot, L. Fan, F. Marquardt, and H. X. Tang, Phys. Rev. Lett. **111**, 213902 (2013).
[13]M. H. Matheny, M. Grau, L. G. Villanueva, R. B. Karabalin, M. C. Cross, and M. L. Roukes, Phys. Rev. Lett. **112**, 014101 (2014).
[14]S. Y. Shah, M. Zhang, R. Rand, and M. Lipson, Phys. Rev. Lett. **114**, 113602 (2015).
[15]M. Zhang, S. Shah, J. Cardenas, and M. Lipson, Phys. Rev. Lett. **115**, 163902 (2015).
[16]T. Li, T.-Y. Bao, Y.-L. Zhang, C.-L. Zou, X.-B. Zou, and G.-C. Guo, Opt. Express **24**, 12336 (2016).
[17]K. Shlomi, D. Yuvaraj, I. Baskin, O. Suchoi, R. Winik, and E. Buks, Phys. Rev. E **91**, 032910 (2015).
[18]L. Ying, Y.-C. Lai, and C. Grebogi, Phys. Rev. A **90**, 053810 (2014).
[19]T. Weiss, A. Kronwald, and F. Marquardt, New J. Phys. **18**, 013043 (2016).
[20]Y.-C. Liu, Y.-F. Xiao, X. Luan, Q. Gong, and C. W. Wong, Phys. Rev. A **91**, 033818 (2015).
[21]Y.-C. Liu, X. Luan, Y.-F. Xiao, and C. W. Wong, Phys. Rev. Lett. **110**, 153606 (2013).
[22]Y. Li, J. Zheng, J. Gao, J. Shu, M. S. Aras, and C. W. Wong, Opt. Express **18**, 23844 (2010).
[23]J. Zheng, Y. Li, M. S. Aras, A. Stein, K. L. Shepard, and C. W. Wong, Appl. Phys. Lett. **100**, 211908 (2012).
[24]J. Zheng, Y. Li, N. Goldberg, M. McDonald, A. Hati, M. Lu, S. Strauf, T. Zelevinsky, D. A. Howe, and C. W. Wong, Appl. Phys. Lett. **102**, 141117 (2013).
[25]X. Luan, Y. Huang, Y. Li, J. F. McMillan, J. Zheng, S.-W. Huang, P.-C. Hsieh, T. Gu, D. Wang, A. Hati, D. A. Howe, G. Wen, M. Yu, G. Lo, D.-L. Kwong, and C. W. Wong, Sci. Rep. **4**, 6842 (2014).
[26]M. Aspelmeyer, T. J. Kippenberg, and F. Marquardt, Rev. Mod. Phys. **86**, 1391 (2014).
[27]J. Wu, S.-W. Huang, Y. Huang, H. Zhou, J. Yang, J.-M. Liu, M. Yu, G. Lo, D.-L. Kwong, G. Xia, and C. W. Wong, *CLEO: Science and Innovations* (Optical Society of America, 2016), p. STu4E.5.
[28]D. Navarro-Urrios, N. E. Capuj, J. Gomis-Bresco, F. Alzina, A. Pitanti, A. Griol, A. Martïnez, and C. M. S. Torres, Sci. Rep. **5**, 15733 (2015).
[29]J. Yang, T. Gu, J. Zheng, M. Yu, G.-Q. Lo, D.-L. Kwong, and C. W. Wong, Appl. Phys. Lett. **104**, 061104 (2014).
[30]E. Rubiola, *Phase Noise and Frequency Stability in Oscillators* (Cambridge University Press, New York, 2008).